

Full Length Research Paper

Laminar and turbulent power law fluid flow passing a square cylinder

Izadpanah Ehsan*, Sefid Mohammad, Nazari Mohammad Reza and Jafarizade Ali

Department of Mechanical Engineering, Yazd University, Yazd, Iran.

Accepted 04 January, 2012

In this work, a two-dimensional laminar and turbulent Power law fluid flow passing a square cylinder is numerically investigated. In the investigation, a finite volume code based on the SIMPLEC algorithm and non-staggered grid was used. In the discretization of the convective and diffusive terms, the third-order QUICK and the second-order central difference scheme, respectively were used. The turbulent flow was simulated using the $k-\omega-\overline{v^2}-f$ model. Extensive numerical results of the drag coefficient, root mean square of the lift coefficient, Strouhal number, stream functions, pressure coefficient, time-averaged velocities and power law viscosity are presented to determine the influence of the Power law index and Reynolds number. Laminar flows discussed in the present work are within the ranges: $60 \leq Re \leq 160$ and $0.6 \leq n \leq 1.6$ covering shear thinning, Newtonian and shear thickening fluids. Turbulent flows within the ranges of $Re=13000$ and 22000 and $0.6 \leq n \leq 1.6$ were also evaluated numerically and discussed.

Key words: Single square cylinder, turbulence $k-\omega-\overline{v^2}-f$ modeling, power law fluid, lift and drag coefficients, Strouhal number.

INTRODUCTION

In recent years, Newtonian fluid flow passing bluff bodies, especially cylinders have been considered because of its vast application and various flow regimes. Some of its industrial applications are: flows over bridges, tall buildings, pipelines, cooling towers and heat exchangers. Numerous investigations have been carried out on the effects of increasing Reynolds number on vortex shedding, the lift and drag coefficients and Strouhal number. Zdravkovich (1997, 2003) presented an extensive review of researches made on the flow passing circular cylinders until 2003. Okajima (1982, 1990) investigated the unconfined Newtonian fluid flow passing a rectangular cylinder experimentally and numerically in the range of $100 \leq Re \leq 20000$ to determine the vortex shedding frequency and Strouhal number. Many

comprehensive studies on both laminar and turbulent Newtonian fluid flows around square cylinders have been conducted by Sohankar et al. (1997, 2000, 2006). In spite of non-Newtonian fluid diversity and its extensive application in food, pharmaceutical, polymer and solution industries and production processes, a few studies have been performed on non-Newtonian fluid flows around cylinders and Newtonian fluids have mostly been considered for this field. Coelho and Pinho (2003a, b) have made experimental investigations on vortex shedding and onset for various regimes of non-Newtonian fluid flows passing a circular cylinder in the range of $50 \leq Re \leq 9000$. Paliwal et al. (2003) have simulated two-dimensional steady state laminar flow with heat transfer around a square cylinder for non-Newtonian fluids in the range of $0.5 \leq n \leq 1.4$, $5 \leq Pe \leq 400$ and $5 \leq Re \leq 40$ numerically to determine the effects of Power law index, Peclet and Reynolds numbers, thermal boundary condition on drag coefficient and Nusselt number. They concluded that the shear thinning fluid do

*Corresponding author. E-mail: izadpanah_ehsan@yahoo.com.
Tel: +98 913 3570349. Fax: +98 351 8210699.

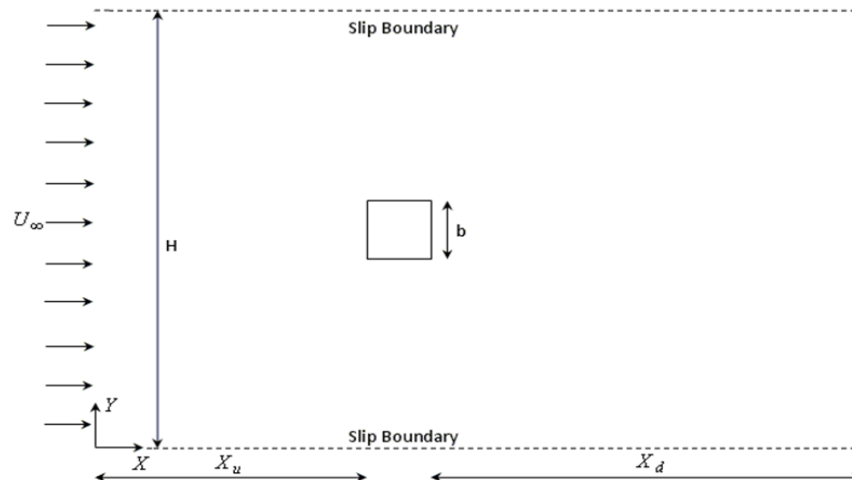


Figure 1. Schematics of the flow around a square cylinder.

not only reduces the size of the wake region but also delays the wake formation, and shear thickening behavior shows the opposite effect.

Dhiman et al. (2008) numerically studied the effects of blockage ratio, $\beta = b/H$, (the ratio of cylinder width, b , to the vertical distance between the top and bottom boundaries, H), Reynolds number ($1 \leq Re \leq 45$) and Power law index ($0.5 \leq n \leq 2.0$) on the flow around a confined square cylinder. It was observed that recirculation length increases linearly with increasing Reynolds number and Power law index, and decreases with increasing blockage ratio. The vortex shedding phenomenon for non-Newtonian fluid flow around a square cylinder in the range of $60 \leq Re \leq 160$ was investigated by Sahu et al. (2009, 2010). Bouaziz et al. (2010) studied non-Newtonian fluid flows around a square cylinder with heat transfer using finite element method. They have also investigated the bouncy effects on heat transfer and flow patterns for Power law fluids. Based on the above references, most studies have been focused on laminar flows of Power law fluids past square cylinders and turbulent flows disregarded. Therefore, in the present research, the effects of the Power law index and Reynolds number on the global parameters of the laminar and turbulent flow such as pressure coefficient, drag and lift coefficients, and Strouhal number are studied numerically using the finite volume method and the turbulence $k - \omega - \overline{v^2} - f$ model.

PROBLEM STATEMENT AND FORMULATION

In this research, incompressible laminar and turbulent flow of non-Newtonian fluid passing an unconfined square cylinder are studied numerically by considering artificial boundaries around the cylinder as shown in Figure 1. For top and bottom boundary conditions, slip

flow boundaries were used. Sohankar et al. (1998) studied the effects of blockage ratio and downstream extent, X_d , on the flow around cylinder. They concluded that for $\beta = 0.05$ and $X_d = 15b$, the distance between the boundaries has minimum effect on it. Based on these results, the variables used in this work were chosen to be $H = 20b$, $X_d = 15b$ and $X_u = 10b$, where X_u is upstream length. Unsteady flow was considered in this study because the vortex shedding occurs at this range of Reynolds number. The governing equations are as follows:

$$\text{Continuity equation: } \nabla \cdot V = 0 \quad (1)$$

$$\text{Momentum equation: } \rho \left(\frac{DV}{Dt} \right) = \nabla \cdot T \quad (2)$$

Where T is total stress tensor and $\frac{DV}{Dt}$ is material derivative of the velocity vector.

$$T = -P\delta + \tau \quad (3)$$

$$\frac{DV}{Dt} = \frac{\partial V}{\partial t} + V \cdot \nabla V \quad (4)$$

Where δ is the unit tensor and P is the static pressure.

Laminar flow

For an incompressible Newtonian fluid, the relationship between shear rate and shear stress can be expressed as follows:

$$\tau_{ij} = 2\mu \varepsilon_{ij} \quad (5)$$

In Equation 5, μ , τ_{ij} and $\varepsilon_{ij} = 1/2(\partial u/\partial y + \partial v/\partial x)$ are viscosity, the components of the stress and of the rate of deformation tensor, respectively. The simplest and often a very useful relationship between shear rate and shear stress for shear

thinning or thickening fluids can be expressed by the Power law model. This relationship can be expressed as follows:

$$\tau_{ij} = 2\eta \varepsilon_{ij}, \quad \eta = m(2\varepsilon_{ij} \cdot \varepsilon_{ji})^{\frac{n-1}{n}} \quad (6)$$

Where η , m and n are the Power law viscosity, the consistency factor and the Power law index, respectively. According to Power law model, if $n < 1$ fluid is shear-thinning, $n = 1$ fluid is Newtonian and $n > 1$ fluid is shear-thickening.

Turbulent flow

For turbulent flows, the instantaneous quantities such as velocity can be separated into a mean value that contains periodic fluctuation and stochastic turbulent fluctuation. Replacing these values in the momentum equations, averaged equations are obtained containing products of turbulent velocity fluctuations. Therefore, a new stress tensor for turbulent flow fields can be written with tensorial notation as follows:

$$T = -P\delta + \tau - \rho Q \quad (7)$$

Where $Q = \overline{v'v'}$ is the velocity fluctuation correlation tensor. These new turbulent stresses that appear in the momentum equations are termed as Reynolds stress and can be simulated by invoking the Boussinesq turbulent stress-strain relationship as follows:

$$-\rho \overline{v'v'} = 2\rho \nu_t \varepsilon_{ij} - \frac{2}{3} \rho k \delta_{ij} \quad (8)$$

Where k is the turbulent kinetic energy. In Equation 8, ν_t is the eddy viscosity that can be simulated using different turbulence models, for example, $k - \omega$ and $k - \varepsilon$.

In recent years, the $\overline{v^2} - f$ turbulence model has become increasingly popular due to its good performance in correctly accounting for nearby wall damping without use of damping functions. Most of $\overline{v^2} - f$ models are based on the $k - \varepsilon$ model. In the present work, the modified $\overline{v^2} - f$ model based on the standard $k - \omega$ model was employed as proposed by Nazari et al. (2009).

The validity of $\overline{v^2} - f$ model has been reported for several applications such as aerodynamics, flow around bluff bodies, separated flow and three-dimensional boundary layers (Lien et al., 1997; Manceau et al., 2000; Iaccarino et al., 2003). The equations used in solving the above mentioned model are presented in Equations 9 to 12.

$$\frac{\partial k}{\partial t} + U_j \frac{\partial k}{\partial x_j} = \frac{\partial}{\partial x_j} \left[\left(\nu_{ap} + \frac{\nu_t}{\sigma_k} \right) \frac{\partial k}{\partial x_j} \right] + P_k - \beta^* \omega k \quad (9)$$

$$\frac{\partial \omega}{\partial t} + U_j \frac{\partial \omega}{\partial x_j} = \frac{\partial}{\partial x_j} \left[\left(\nu_{ap} + \frac{\nu_t}{\sigma_\omega} \right) \frac{\partial \omega}{\partial x_j} \right] + \zeta \frac{\omega}{k} P_k - \beta \omega^2 \quad (10)$$

$$\frac{\partial \overline{v^2}}{\partial t} + U_j \frac{\partial \overline{v^2}}{\partial x_j} = \frac{\partial}{\partial x_j} \left[\left(\nu_{ap} + \frac{\nu_t}{\sigma_{v^2}} \right) \frac{\partial \overline{v^2}}{\partial x_j} \right] + kf - 6\overline{v^2} \beta^* \omega \quad (11)$$

$$L^2 \frac{\partial^2 f}{\partial x_j^2} - f = \frac{C_1}{T} \left(\frac{\overline{v^2}}{k} - \frac{2}{3} \right) - C_2 \frac{P_k}{k} - \frac{1}{T} \left(6 \frac{\overline{v^2}}{k} - \frac{2}{3} \right) \quad (12)$$

Where $\nu_{ap} = \eta / \rho$, $\nu_t = \min \{ k / \omega, C_\mu \overline{v^2} T \}$ and $P_k = 2\nu_t S_{ij} S_{ij}$ are apparent viscosity, the eddy viscosity and the production of the kinetic energy, respectively. The time scale and length scale are $T = \max \{ 1 / \beta^* \omega, C_\zeta \sqrt{\nu_{ap} / \beta^* \omega k} \}$, $L = C_l \max \{ k^{0.5} / \beta^* \omega, C_\eta \nu^{0.75} / (\beta^* \omega k)^{0.25} \}$ the model constants are $\beta^* = 0.09$, $C_\mu = 0.27$, $\sigma_\omega = 1.0$, $\sigma_k = 2.0$, $C_1 = 1.4$, $C_2 = 0.3$, $C_l = 0.5$, $C_\eta = 15.0$, $C_\zeta = 0.5$, $\beta = 0.075$, $\zeta = 5/9$. All parameter and constants are adopted from Nazari et al. (2009).

Boundary conditions

A uniform flow was considered at the inlet and as of the outlet a convective boundary condition (Orlanski condition) was used for all velocity components. No slip conditions have been prescribed at the cylinder surfaces. Symmetry conditions which represent slip boundary conditions were used at the upper and lower boundaries. The boundary conditions are chosen as shown in Equations 13 to 16.

Inlet: $u = U_\infty = 1, v = 0 \quad (13)$

Cylinder surfaces: $u = v = 0 \quad (14)$

Outlet: $\frac{\partial \varphi}{\partial t} + U_c \frac{\partial \varphi}{\partial x} = 0 \quad (15)$

Symmetry: $\frac{\partial u}{\partial y} = 0, v = 0 \quad (16)$

Using the Orlanski boundary condition, the value of U_c is set to U_∞ . Boundary conditions at the solid walls for $k - \omega - \overline{v^2} - f$ model are $k = \overline{v^2} = f = 0$ and $\omega = 6\nu_{ap} / \beta y^2$. The values of X_u , X_d and H are set to 10, 15 and 20b, respectively (Figure 1). The instantaneous values of the drag and lift coefficients on the cylinder can be calculated at each time step and are defined as stated in Equations 17 to 18.

$$C_D = \frac{F_D}{1/2 \rho U_\infty^2 b} \quad (17)$$

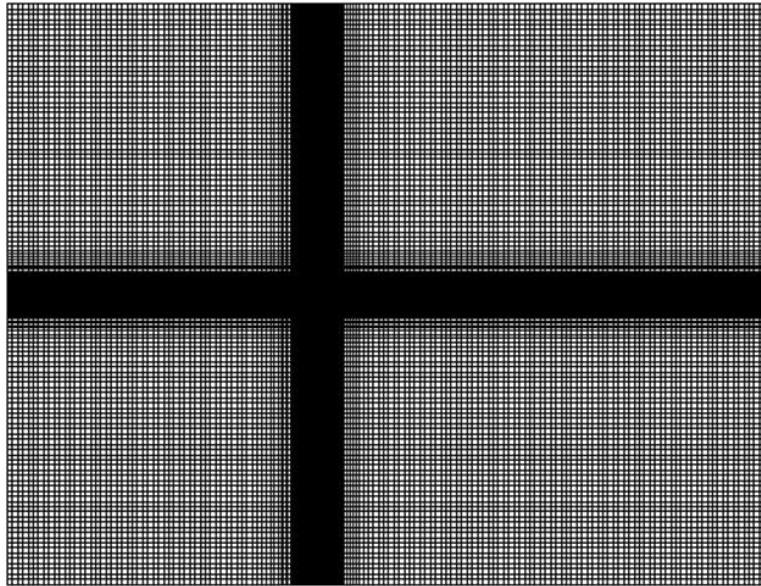


Figure 2. Non-uniform computational grid (202 × 236).

$$C_L = \frac{F_L}{1/2 \rho U_\infty^2 b} \quad (18)$$

Where F_D and F_L are the drag and lift forces exerted by the fluid on the cylinder, respectively. These forces are calculated by integrating the viscous shear forces and pressure over the surface of the cylinder. The Reynolds and Strouhal number are defined as expressed in Equations 19 to 20.

$$Re = \frac{\rho U_\infty^{2-n} b^n}{m} \quad (19)$$

$$St = \frac{f b}{U_\infty} \quad (20)$$

Where f is the vortex shedding frequency.

Numerical method

Presented results in this work are obtained numerically by an incompressible finite volume CALC-BFC code using collocated grid arrangement developed. The SIMPLEX algorithm has been used for pressure-velocity coupling. However, for time discretization the second order Crank–Nicolson scheme was used. The third-order QUICK and central difference schemes were considered to discretize convective and diffusive terms, respectively. The time step is set at 0.005 for both laminar and turbulent states as smaller values do not have any significant effect on numerical accuracy or stability. More details about the code can be found in Sohankar et al. (1996).

RESULTS AND DISCUSSION

In this work, numerical computations are carried out for

both laminar and turbulent non-Newtonian fluid flows. Laminar flows in the range of $60 \leq Re \leq 160$ and $0.6 \leq n \leq 1.6$ that covers shear thinning, Newtonian and shear thickening fluids are discussed. Also turbulent flows for $Re=13000$ and 22000 and $0.6 \leq n \leq 1.6$ are studied numerically. The effect of the Power law index and Reynolds number on flow characteristics such as lift and drag coefficients, Strouhal number, pressure coefficient, time-averaged velocity and Power law viscosity are investigated.

Grid independence

Grid size is a considerable parameter in numerical methods. Grid size and number of control volumes influence the calculation time of the code and the result error. It would thus be very good to obtain grid independent results. In the present work, a non-uniform grid was used around the cylinder in the flow field. The meshing was split in five regions each having different number of nodes as shown in Figure 2. These grids are produced by hyperbolic tangent distribution functions. In this study, seven different grids were used to investigate the effects of the grids on the results of laminar and turbulent flows. For laminar flows, grid D was chosen. If $y^+ = \rho w^{2-n} y^n / k$, dimensionless wall distance of the nearest node to the cylinder is less than one, satisfactory results can be obtained for turbulent flows. In y^+ equation, $w = \sqrt{\tau_w / \rho}$ is the friction velocity and τ_w is the wall shear stress. For turbulent flows, grid E was adopted.

Table 1. Validating laminar flow characteristics.

<i>Re</i>	<i>n</i>	Source	C_D	C_{DP}	C_{Lrms}	<i>St</i>
60	0.7	Present	1.44	1.33	0.052	0.136
60	0.7	Sahu et al. (2009)	1.46	1.41	0.083	0.136
100	1.0	Present	1.52	1.43	0.177	0.148
100	1.0	Sahu et al. (2009)	1.49	1.44	0.194	0.149
160	1.6	Present	1.79	1.61	0.294	0.146
160	1.6	Sahu et al. (2009)	1.68	1.53	0.262	0.147
200	1.0	Present	1.41	1.49	0.250	0.168
200	1.0	Sohankar et al. (1998)	1.43	1.47	0.229	0.165

Table 2. Comparison turbulent flow.

<i>Re</i>	<i>n</i>	Grid/Source	Grid resolution	C_D	C_{DP}	C_{Lrms}	<i>St</i>
13000	1.0	A	92×107	1.962	1.982	0.999	0.148
13000	1.0	B	114×131	1.974	1.989	0.998	0.147
13000	1.0	C	118×139	1.978	1.993	1.008	0.146
13000	1.0	D	124×144	1.967	1.980	0.956	0.148
13000	1.0	E	132×152	2.028	2.041	1.122	0.148
13000	1.0	F	134×156	2.066	2.080	1.241	0.148
13000	1.0	G	202×236	2.162	2.174	1.483	0.148
13000	1.0	Norberg (1993)		2.160	-	-	0.132
22000	1.0	A	92×107	1.777	1.790	0.546	0.142
22000	1.0	B	114×131	1.914	1.926	0.833	0.146
22000	1.0	C	118×139	1.927	1.939	0.872	0.146
22000	1.0	D	124×144	1.907	1.918	0.808	0.146
22000	1.0	E	132×152	1.990	2.001	1.010	0.147
22000	1.0	F	134×156	2.028	2.040	1.127	0.147
22000	1.0	G	202×236	2.136	2.147	1.400	0.146
22000	1.0	Lyn et al. (1995)		2.100	-	-	0.130
22000	1.0	Sohankar et al. (2000)		2.320	-	1.540	0.132
22000	1.0	Lubcke et al. (2001)		2.206	-	0.950	0.150

Even though there are many papers specifically about laminar Newtonian and non-Newtonian fluid flows, there are none on turbulent non-Newtonian fluid flows passing square cylinders. Hence, the laminar flow results are compared with available Newtonian and non-Newtonian results for validating the calculations, but turbulent flow validation has been done using Newtonian results. Some of these comparisons are shown in Tables 1 and 2.

Laminar results

In this section, the numerical results for laminar flows are presented. Figure 3 shows time-averaged streamlines around a cylinder for $Re=80$ and 160 and $n=0.6, 0.8, 1.0$ and 1.6 . It is seen that the recirculation length increases

as the Power law index increase or as Reynolds number decrease. As shown in Figure 3a, leading edge separation takes place only for $n=0.6$ and in Figure 3b, it occurs for both $n=0.8$ and 1.0 . Therefore, it can be concluded that leading edge separation for shear thinning fluids takes place for lower Reynolds numbers. Separation from the leading edge results in widening of wake area. It is observed that for a single Reynolds number, there are three kinds of separations; separation from the trailing edges, separation from the leading edge with reattachment and separation from the leading edge without reattachment in the trailing edges. This phenomenon depends on the fluid nature and it affects some flow characteristics, for example, C_L and C_D .

In Figure 4, the drag coefficient variation with respect to Re for different Power law indexes is shown. The drag

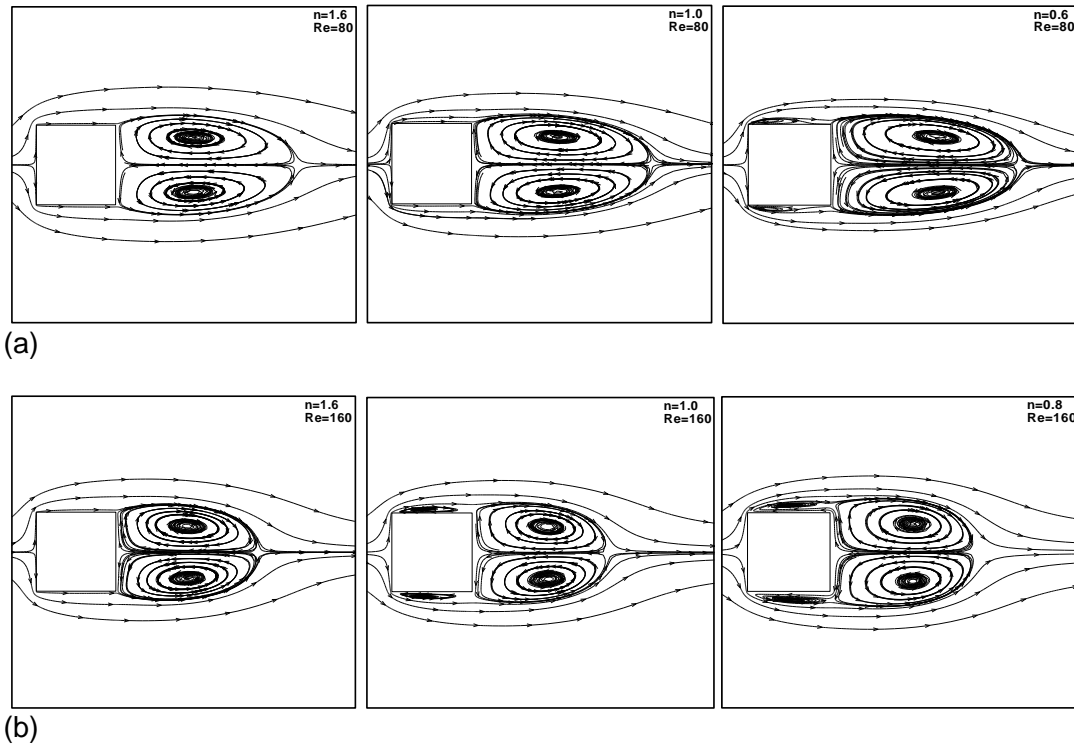


Figure 3. Time averaged streamlines at $Re = 80$ and 160 for $n = 0.6, 0.8, 1.0$ and 1.6 .

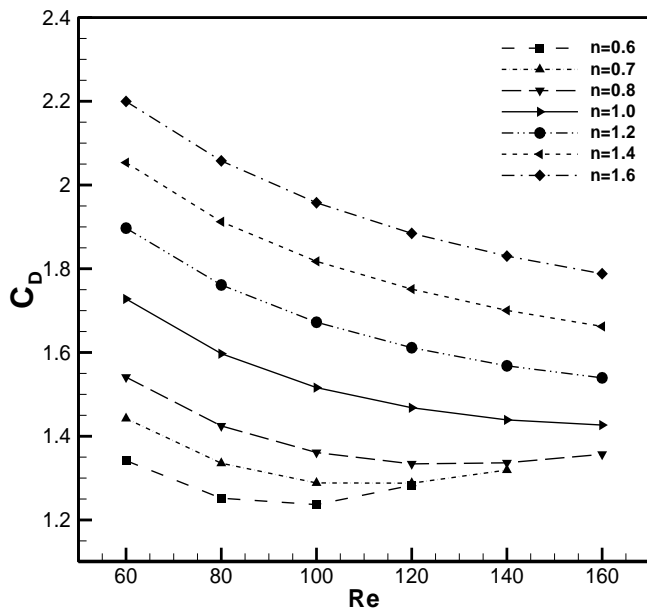


Figure 4. Variation of time-averaged total drag coefficient with Reynolds number for laminar flow (Newtonian and non-Newtonian fluid).

force consists of two components; viscous drag and pressure drag. Viscous drag acts on the top and bottom surfaces of the cylinder, but pressure drag acts on the front and rear surfaces of the cylinder. As shown in

Figure 4 by increasing the Reynolds number, drag coefficient decreases for shear thickening and Newtonian fluids. The same phenomenon is shown for shear thinning fluids up to a certain Reynolds number. Above that specific number, the leading edge separation takes place and the viscous drag becomes negative. As mentioned earlier, leading edge separation without reattachment results in increase of the wake area width. Increasing the wake area width, results in increasing the pressure drag as shown in Figure 5. In other words, leading edge separation causes the viscous drag to become negative and pressure drag to increase. The effect of pressure drag is more than viscous drag. These results in total increase the drag for shear thinning fluids. As known, the wake area is a low pressure area and larger width of wake area leads to larger pressure drag. As leading edge separation width of wake area in shear thinning fluids is larger as compared to Newtonian and shears thickening fluids, wider wake area results in an increase of the pressure drag coefficient gradient.

Figure 6 shows variations of C_{Lrms} , rms value of lift with respect to Reynolds number for different Power law indexes. As shown for all Power law indexes, by increasing Reynolds number, C_{Lrms} increases. The difference between shear thickening and shear thinning fluids is the sharp increase of C_{Lrms} in shear thinning fluids. This phenomenon is due to an increase in the amplitude of C_L which is affected by the widening of the wake area.

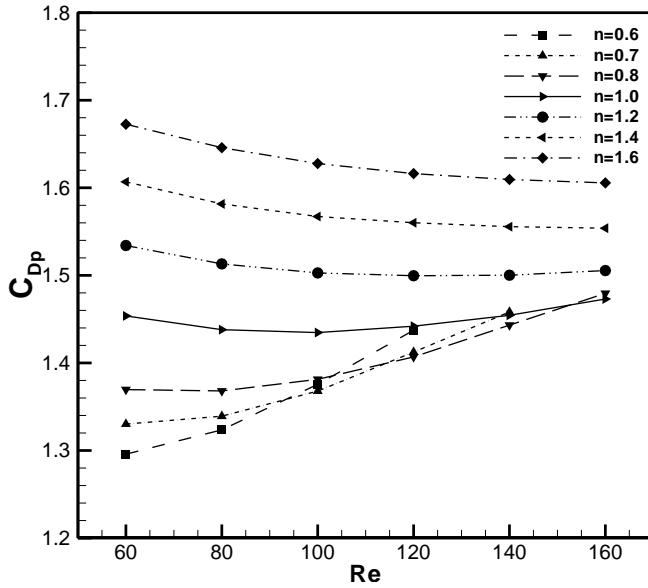


Figure 5. Variation of time-averaged pressure drag coefficient with Reynolds number for laminar flow (Newtonian and non-Newtonian fluid).

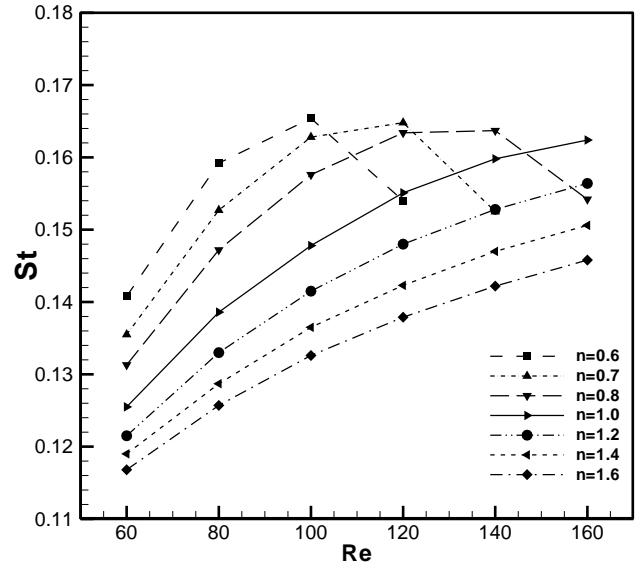


Figure 7. Variation of Strouhal number with Reynolds number for laminar flow (Newtonian and non-Newtonian fluid).

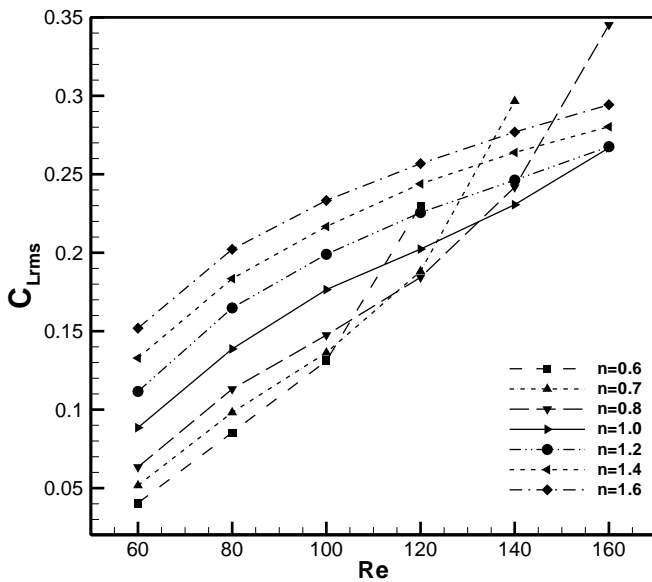


Figure 6. Variation of rms value of lift coefficient with Reynolds number for laminar flow (Newtonian and non-Newtonian fluid).

As shown in Figure 7, increasing Re , results in increasing Strouhal number. After the leading edge separation takes place, this phenomenon becomes inverse and Strouhal number become smaller due to a wider wake area. As shown in Equation 20, Strouhal number is the frequency of vortex shedding and it is proportional with the inverse of time. As the wake area becomes wider, it takes more time for a vortex to shed,

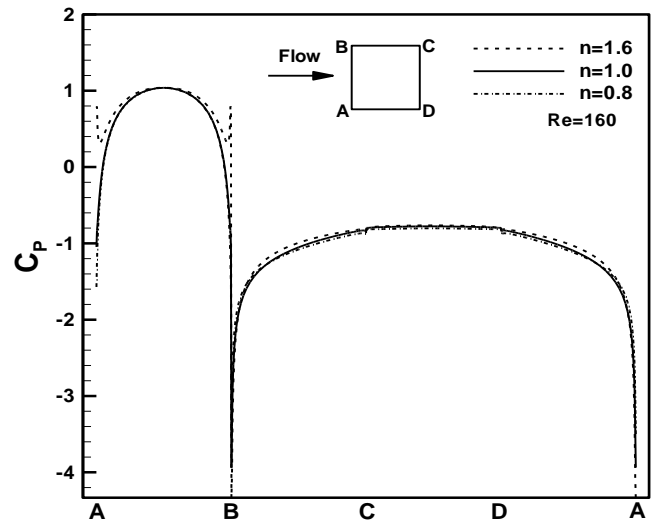


Figure 8. Time-averaged pressure coefficient around the cylinder for laminar flow (Newtonian and non-Newtonian fluid).

which in turn results in a lower Strouhal number. Figure 8 shows the variation of pressure coefficients for $Re=160$ and $n=0.8, 1.0$ and 1.6 . As mentioned earlier, the wake region is a low pressure region. In Figure 8, it is observed that C_p of shear thinning fluids is more negative than corresponding of shear thickening and Newtonian fluids because of formation of wake at the top and bottom sides and extending of this region in the trailing edge of cylinder (region BCDA).

Figures 9 and 10 show time averaged velocity profiles at

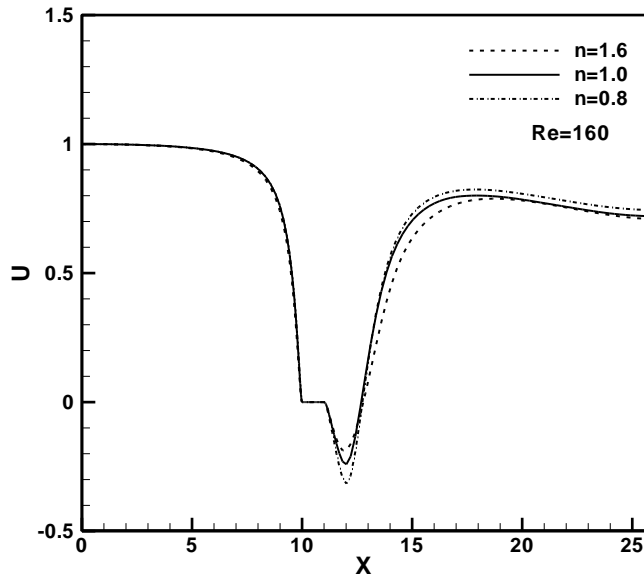


Figure 9. Time-averaged stream wise velocity profiles in the centerline of the cylinder for laminar flow (Newtonian and non-Newtonian fluid).

the centerline and at different cross sections, respectively. Differences between these velocity profiles are due to different kinds of separations, as well as differences in fluid nature. In these figures, recirculation length and recirculation width are obvious.

Figure 11 shows the variation of v_{ap}/U (ratio of Power law viscosity to Newtonian viscosity) around cylinder surfaces for $Re=160$ and $n=0.8$ and 1.6 . It is observed that shear thinning and shear thickening fluids behave inversely. The maximum variations of v_{ap}/U are seen at the cylinder corners and at stagnation points. This phenomenon is due to sharp variations of velocity gradients. As viscosity changes, other flow characteristics also change.

Turbulent results

The numerical results for turbulent flows using $k-\omega-\overline{v^2}-f$ turbulence model, are presented in this section. Figure 12 shows the time-averaged streamlines around a cylinder for $Re=13000$ and 22000 , and $n=0.6$, 1.0 and 1.4 . In contrast to laminar flows, by increasing the Power law index, the recirculation length decreases and by increasing the Reynolds number, the recirculation length increases for all Power law indexes. For turbulent flows, the effect of Power law index on recirculation shape and length is more significant than the effect of Reynolds number. As shown in Figure 12, all Power law indexes and Reynolds numbers leading edge separation

takes place. Therefore the recirculation width is almost constant for all sex cases presented above.

Figures 13 and 14 represents drag coefficient and Strouhal number variations with respect to the Power law index for $Re=13000$ and 22000 , respectively. As shown from these figures, by increasing the Power law index, drag coefficient and Strouhal Number increase and these variations for $Re=13000$ are larger than for $Re=22000$. Figure 15 shows pressure coefficient variations for turbulent flows with $Re=22000$ and $n=0.6$, 1.0 and 1.4 . The results obtained in this work are compared with the experimental results for Newtonian fluids presented by Norberg (1993). As observed, variation of C_p at the top, bottom and rear edges of the cylinder for shear thinning fluids are larger than the corresponding for shear thickening and Newtonian fluids. This phenomenon depends on the wake region formation. Figures 16 and 17 show time-averaged velocity profiles for turbulent flows with $Re=22000$ and $n=0.6$, 1.0 and 1.4 at the centerline and at three different cross sections, respectively. Results are compared with Newtonian fluids solved with Large Eddy Simulation turbulence model, Sohankar et al. (2000) and Sohankar (2006). It is obvious from these figures that the recirculation length for shear thinning is larger than corresponding value for shear thickening. The variation of time-averaged velocity for shear thinning is greater than the corresponding one for shear thickening fluids.

Figure 18 shows variations of v_{ap}/U around the cylinder surface for $Re=13000$ at $n=0.6$ and 1.4 . As for laminar flows, shear thinning and shear thickening fluids behave inversely and the maximum variations of v_{ap}/U are seen at the cylinder corners. By comparing the variations in v_{ap}/U between laminar and turbulent flows, for shear thinning fluids, it is seen that the variation is less for turbulent flows as compared to laminar flows. In contrast to shear thinning, shear thickening fluid variations between laminar and turbulent flows are not significant.

CONCLUSION

Laminar and turbulent Power law fluid flows passing an unconfined single square cylinder by using the $k-\omega-\overline{v^2}-f$ turbulence model were investigated numerically to obtain flow characteristics such as drag coefficient, root mean square of lift coefficient, recirculation length, stream functions, pressure coefficient, time-averaged velocities and Power law viscosity. For laminar flows, the range of Reynolds number and Power law index considered are $Re=60$ and 160 and $0.6 \leq n \leq 1.6$. For turbulent flows discussed, these values are $Re=13000$ and 22000 and

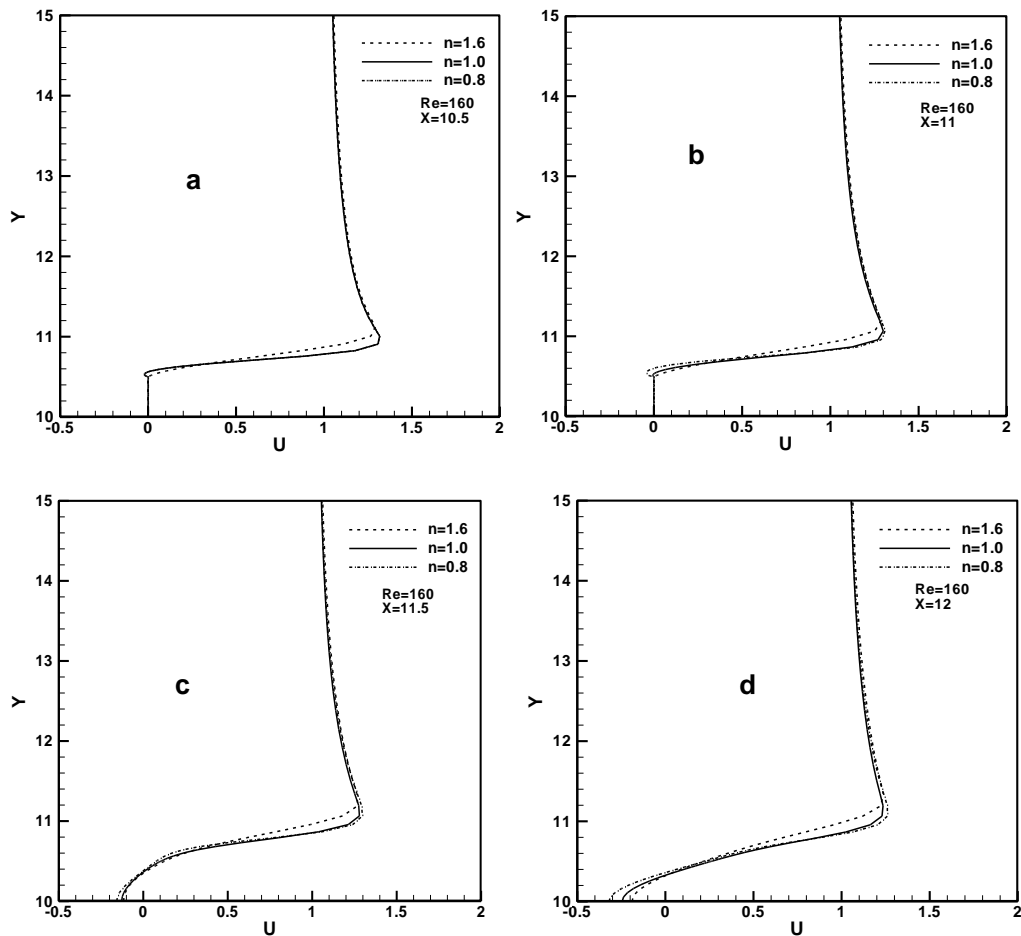


Figure 10. Time-averaged stream wise velocity profiles at four locations for laminar flow (Newtonian and non-Newtonian fluid).

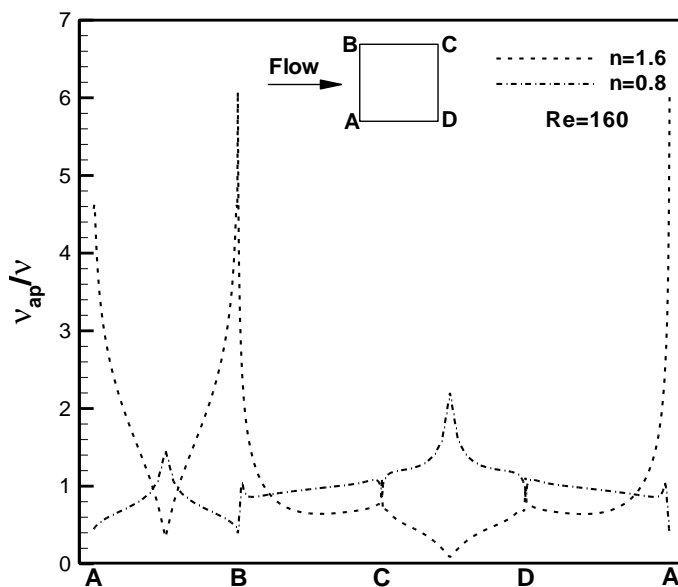


Figure 11. Variation of v_{ap}/v around the cylinder surfaces for $Re=160$ at $n=0.8$ and 1.6 .

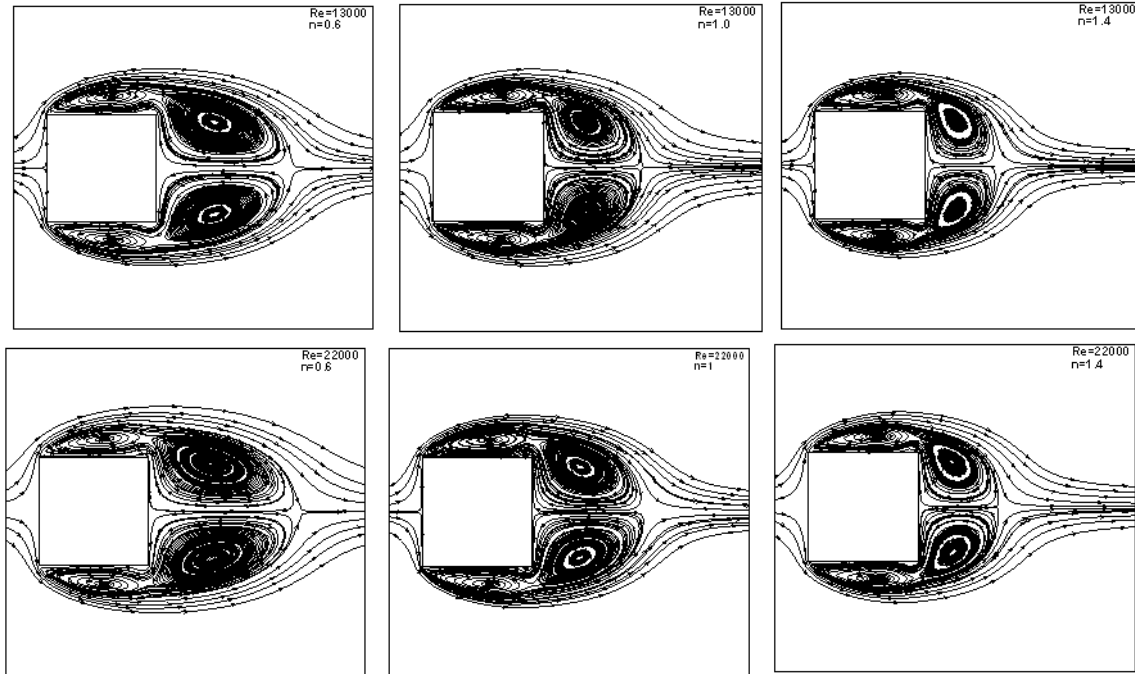


Figure 12. Time averaged streamlines at Re =13000 and 22000 for n = 0.6, 1.0 and 1.4.

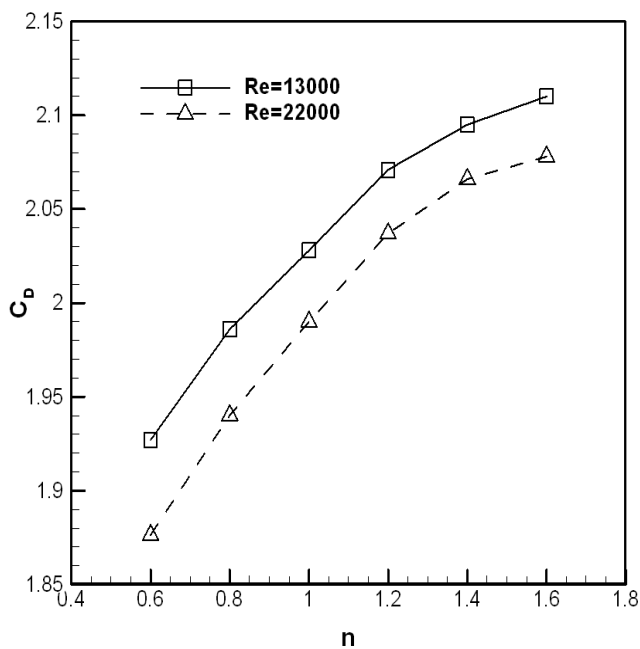


Figure 13. Variation of time-averaged total drag coefficient with Power law index for turbulent flow (Newtonian and non-Newtonian fluid).

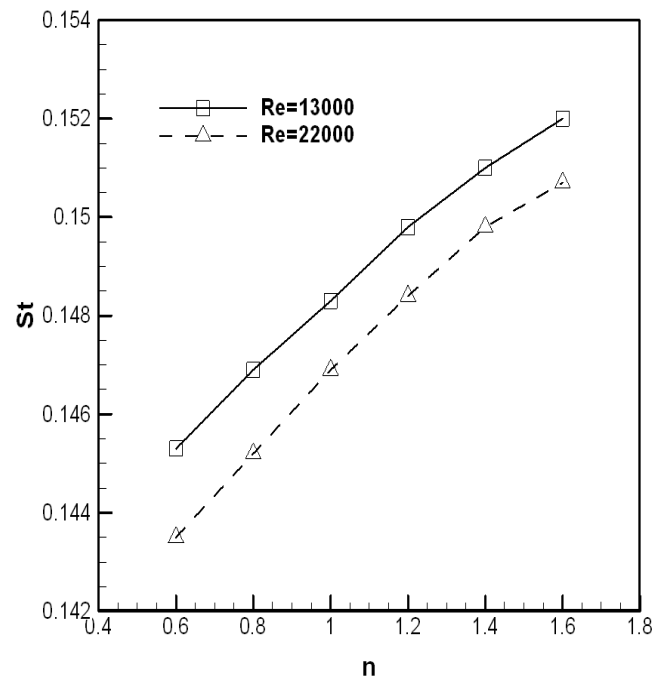


Figure 14. Variation of Strouhal number with Power law index for turbulent flow (Newtonian and non-Newtonian fluid).

$0.6 \leq n \leq 1.6$. This range of Power law index covers shear thinning, Newtonian and shear thickening fluids. For the studied values of Reynolds numbers, the vortex shedding phenomenon occurred. By increasing the

Reynolds number in laminar shear thinning and Newtonian fluid flows, the position of flow separation shifts to the front edge of the cylinder. For shear thickening fluids in the present range of Reynolds number

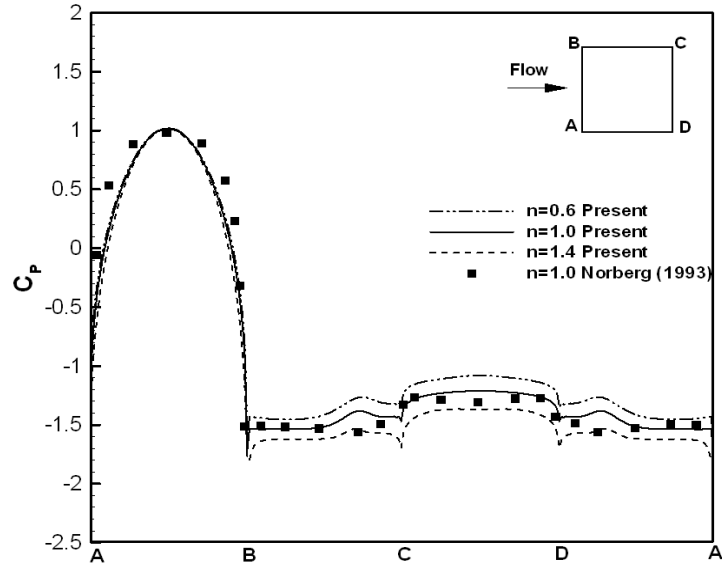


Figure 15. Time-averaged pressure coefficient around the cylinder for turbulent flow (Newtonian and non-Newtonian fluid).

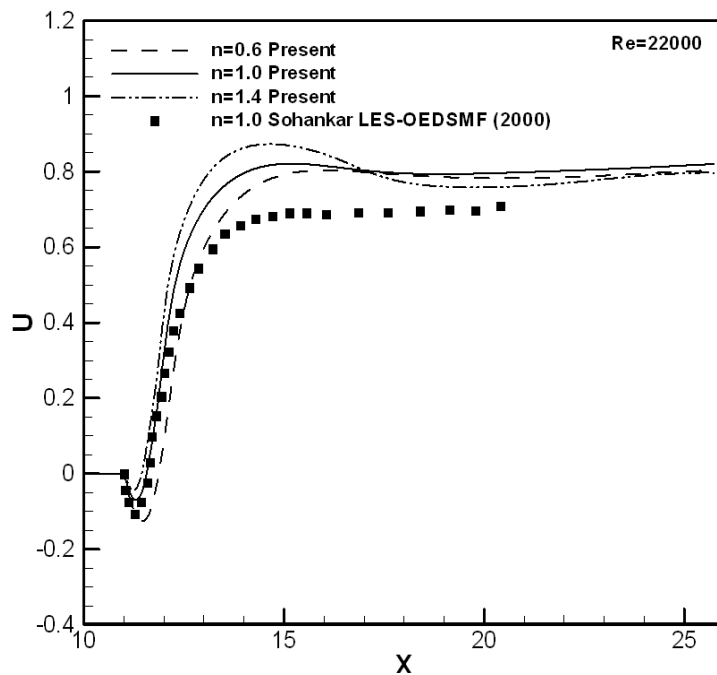


Figure 16. Time-averaged stream wise velocity profiles in the centerline of the cylinder for turbulent flow (Newtonian and non-Newtonian fluid).

and Power law index, there was no leading edge separation. As leading edge separation occurred, the wake width increased as a result of flow behavior changes. This phenomenon has also been reported by Sahu et al. (2009). In the present work, turbulent flows with $Re=13000$ and 22000 in the range of $0.6 \leq n \leq 1.6$

was studied. As the Reynolds numbers are high for all shears thinning, Newtonian and shear thickening fluids, leading edge separation was observed. In contrast to laminar flows, the recirculation length in shear thinning fluids was larger than the corresponding for Newtonian and shears thickening fluids. By comparing the two

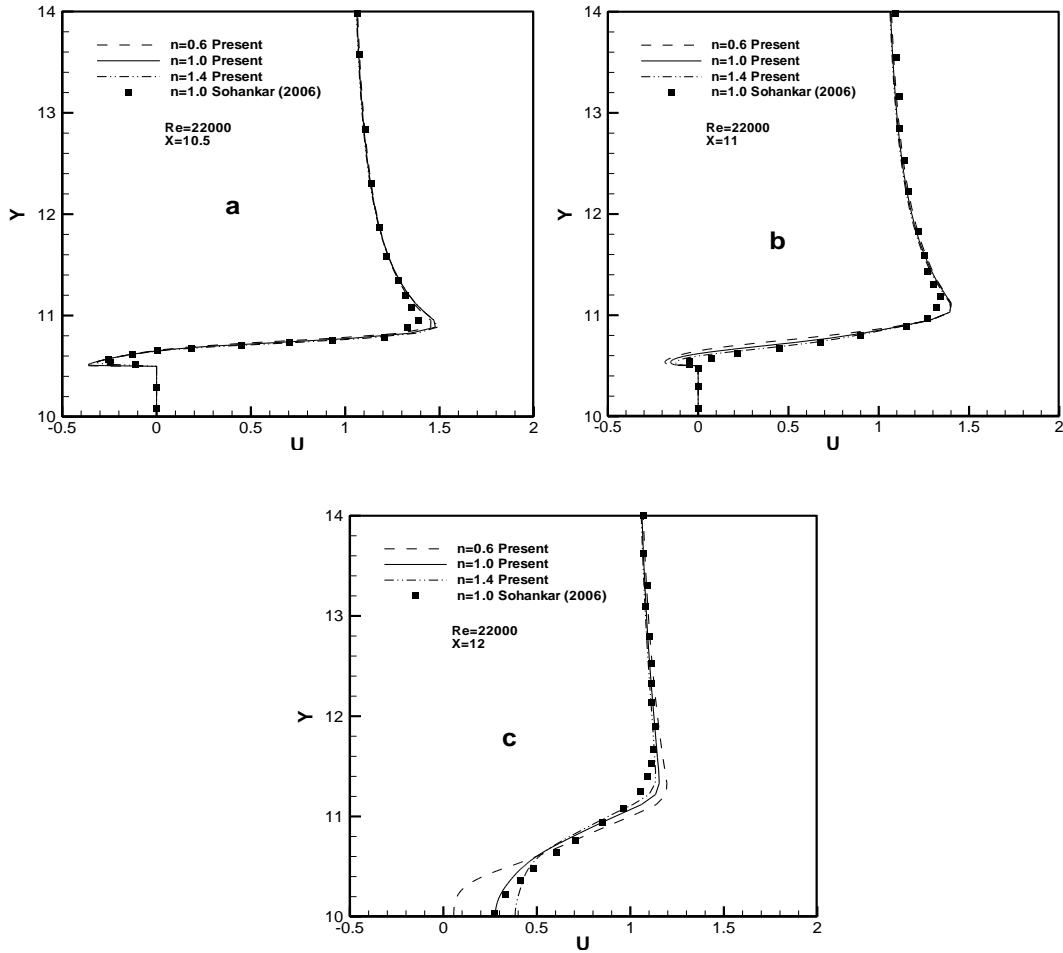


Figure 17. Time-averaged stream wise velocity profiles at three locations for turbulent flow (Newtonian and non-Newtonian fluid).

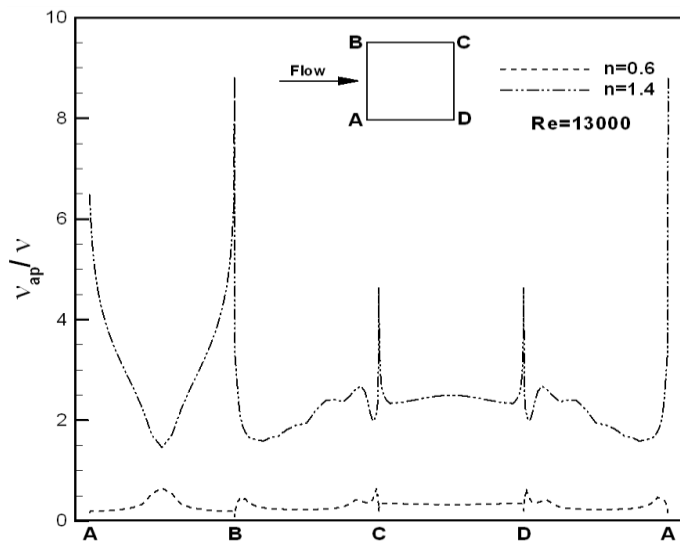


Figure 18. Variation of v_{ap}/v around the cylinder surfaces for $Re=13000$ at $n=0.6$ and 1.4 .

Reynolds numbers in the range of Power law index, it was concluded that the Power law index affected flow characteristics such as recirculation length, stream functions, etc., more than the Reynolds number.

REFERENCES

Bouaziz M, Kessentini S, Turki S (2010). Numerical prediction of flow and heat transfer of Power-law fluids in a plane channel with a built-in heated square cylinder. *Int. J. Heat and Mass Transfer.*, 53: 5420-5429.

Coelho PM, Pinho FT (2003a). Vortex shedding in cylinder flow of shear-thinning fluids I. Identification and demarcation of flow regimes. *J. Non-Newtonian Fluid Mech.*, 110: 143-176.

Coelho PM, Pinho FT (2003b). Vortex shedding in cylinder flow of shear-thinning fluids II. Flow characteristics. *J. Non-Newtonian Fluid Mech.*, 110: 177-193.

Dhiman AK, Chhabra RP, Eswaran V (2008). Steady flow across a confined square cylinder: effects of Power-law index and of blockage ratio. *J. Non-Newtonian Fluid Mech.*, 148: 141-150.

Iaccarino G, Ooi A, Durbin P, Behnia M (2003). Reynolds averaged simulation of unsteady separated flow. *Int. J. Heat Fluid Flow*, 24: 147-156.

- Lien FS, Durbin PA, Parneix S (1997). Non-linear $\overline{v^2} - f$ modeling with application to aerodynamic flows. Proceeding of the 11th Symposium Turbulent shear flows, Grenoble, France, pp. 8–10.
- Lubcke H, Schmidt S, Rung T, Thiele F (2001). Comparison of LES and RANS in bluff-body flows. *J. Wind Eng. Ind. Aerodyn.*, 89: 1471–1485.
- Lyn DA, Einav S, Rodi W, Park JH (1995). A laser-Doppler velocimetry study of ensemble-averaged characteristics of the turbulent near wake of a square cylinder. *J. Fluid Mech.*, 304: 285–319.
- Manceau R, Parneix S, Laurence D (2000). $\overline{v^2} - f$ Turbulent heat transfer predictions using the $\overline{v^2} - f$ model on unstructured meshes. *Int. J. Heat Fluid Flow*, 21: 320–328
- Nazari MR, Sohankar A, Malekzadeh S, Alemrajabi A (2009). Reynolds-averaged Navier–Stokes simulations of unsteady separated flow using the $k - \omega - \overline{v^2} - f$ model. *J. Turbulencem* 10: 1–13.
- Norberg C (1993). Flow around rectangular cylinders: Pressure Forces and Wake Frequencies. *J. Wind Eng. Ind. Aerodyn.*, 49: 187–196.
- Okajima A (1982). Strouhal numbers of rectangular cylinders. *J. Fluid Mech.*, 123: 379–398.
- Okajima A (1990). Numerical simulation of flow around rectangular cylinders. *J. Wind Eng. Ind. Aerodyn.*, 33: 171–180.
- Paliwal B, Sharma A, Chhabra RP, Eswaran V (2003). Power law fluid flow past a square cylinder: momentum and heat transfer characteristics. *Chem. Eng. Sci.*, 58: 5315–5329.
- Sahu AK, Chhabra RP, Eswaran V (2009). Two-dimensional unsteady laminar flow of a Power law fluid across a square cylinder. *J. Non-Newtonian Fluid Mech.*, 160: 157–167.
- Sahu AK, Chhabra RP, Eswaran V (2010). Two-dimensional laminar flow of a Power-law fluid across a confined square cylinder. *J. Non-Newtonian Fluid Mech.*, 165: 752–763.
- Sohankar A (2006). Flow over a bluff body from moderate to high Reynolds numbers using large eddy simulation. *Comp. Fluids*, 35: 1154–1168.
- Sohankar A, Norberg C, Davidson L (1997). Numerical simulation of unsteady low-Reynolds number flow around rectangular cylinders at incidence. *J. Wind Eng. Ind. Aerodyn.*, 69: 189–201.
- Sohankar A, Norberg C, Davidson L (1998). Low-Reynolds number flow around a square cylinder at incidence: study of blockage, onset of vortex shedding and outlet boundary condition. *Int. J. Num. Meth. Fluids*, 26: 39–56.
- Sohankar A, Norberg C, Davidson L (2000). Large eddy simulation of flow past a square cylinder: comparison of different subgrid scale models. *ASME J. Fluids Eng.*, 122: 39–47.
- Zdravkovich MM (1997). *Flow Around Circular Cylinders*, Vol. 1, Fundamentals. Oxford University Press, New York, 694 p.
- Zdravkovich MM (2003). *Flow Around Circular Cylinders*, Vol. 2, Applications. Oxford University Press, New York, 692 p.